

ORIGINAL RESEARCH PAPER

Effect of pH variation on Bandgap and Visible Light Photocatalytic Properties of TiO₂ Nanoparticles

R.Sarathi^{1*}, S.Meenakshi Sundar²

¹ Research Scholar, (Reg.No: 19111232132001) PG and Research Department of Physics, Sri Paramakalyani College Alwarkurichi Affiliated to Manonmaniam Sundaranar University, Abishekapatti, Tirunelveli-627012, Tamilnadu, India.

² Principal, Sri Paramakalyani College Alwarkurichi-627412.

Received: 2022-05-21

Accepted: 2022-06-26

Published: 2022-07-01

ABSTRACT

Titanium-di-oxide nanoparticles are synthesized via a microwave-assisted solvothermal route for different pH values. The effect of the acidic and basic nature of the solvent due to the pH value is reflected in the crystalline size of the compound. The purpose of this work is to synthesize Titanium dioxide nanoparticles and to observe their application in degrading industrially contaminated water using normal tap water. The crystalline sizes are calculated using XRD analysis and confirmed with HRTEM. The chemical composition and oxidation state are confirmed with XPS studies. Optical properties are carried out with UV-Vis, FTIR, and PL spectra. Photocatalytic studies are carried out to degrade the dye in industrial water. The efficiency of degradation is calculated with the UV-Vis data and formula. The reduction in band gap and high permanence has greatly supported in making it acceptable for photocatalytic activity under visible light. Dependence of time, initial dye concentration, and pH of the dye solution on TiO₂ as a catalyst is investigated under the illumination of a visible lamp, and degradation efficiency to the highest of 96.79% has been obtained.

Keywords: Microwave Irradiation Method, Titanium dioxide, Photocatalysis, Reuse, Malachite Green Dye

How to cite this article

Sarathi R., Meenakshi Sundar S. Effect of pH variation on Bandgap and Visible Light Photocatalytic Properties of TiO₂ Nanoparticles. J. Water Environ. Nanotechnol., 2022; 7(3): 252-266.
DOI: 10.22090/jwent.2022.03.003

INTRODUCTION

Nanoscience is a convergence of Physics, materials science, and biology, which deal with the manipulation of materials at atomic and molecular scales, while nanotechnology is the ability to observe, measure, manipulate, assemble, control, and manufacture matter at the nanometer scale. Nanotechnology deals with the use of nanomaterials for pragmatic applications for society-based projects and projects for sophisticated lifestyles. They are studied because of their size-dependent physical and chemical properties. Various industries like fabric, mat, wrapper, comestible, beauty-product, and pharmaceuticals industries use multiple ranges

of colors for selling their materials to us [1]. These industries use colored dyes for their products. Dyes are naturally available or synthetic compounds that make permanent color to fabric, reed mats, cosmetics, etc. [2] Based upon their composition, dyes are categorized as acid dyes, direct dyes, azo dyes, disperse dyes, sulfur dyes, fiber reactive dyes, basic dyes, oxidation dyes, mordant dyes, developed dyes, vat dyes, pigments, fluorescence or optical brighteners and solvent dyes [3]. These toxic dyes lead to severe health issues in living organisms. All these industries, after making use of the dyes, dispose of them as waste in nature.

Nature never disturbs the qualities of water, light, and air. But it may cause damage to the

* Corresponding Author Email: sarathi.tuty@gmail.com

infrastructure as a whole. Contamination of water bodies by human create a great disaster in our ecosystem and also for the living organisms. In most developing countries water contamination and the availability of clean water for human consumption is a leading problem [4]. An increase in population is also one of the reasons for water scarcity. In that view, the human need has made the water resources more tainted and the shortage of drinking water sources prevails [5]. Water resources for livestock production, all-year-round irrigation, and other agricultural activities are highly altered due to contamination by human activities like discharging industrial waste to water bodies [6]. The main component of this outflow of dyestuff is from the industries like food beverages, printing, plastics, paints, leather, and cosmetics [7]. They use a large quantity of fresh water and reverse it into an enormous amount of wastewater and make this poisonous and disagreeable waste to mix with the water bodies [8]. These dye wastes are adverse causing mucous membrane irritation, eye irritation, skin irritation, contact dermatitis, respiratory diseases and even carcinogenic to humans dyes on the surface of the water affect the living organism in water, photosynthesis in aquatic plants blocking penetration of sunlight [9]. Several areas of basic and applied research are concerned with removing dye from industrial waste [10]. Various methods like adsorption using dead/ living microbial biomass, degradation by white-rot fungi, using sodium hypochlorite, membrane filtration, electrokinetic coagulation, and adsorption by activated carbon. Though these methods can degrade toxic dyes they have some drawbacks such as high waste production, not applying to all dyes, very costly, short half-life, etc. [11]. Compared to all other methods photocatalysis is a prominent method for degrading dyes because its by-products i.e., mineral acids, carbon-di-oxide, and water are harmless. [12].

Some of the previous works for the same are as follows, Sayadi MH et al., (2022) have synthesized ZnO/SnO₂ nanoparticles and studied its photocatalytic degradation of Congo red, Biphenyl A, and tetracycline with 5 ppm dye concentration and 0.5g of photocatalyst [13]. Poorsajadi et al., (2021) synthesized copper-supported Bismuth oxide nanoparticles and observed its decolorization effect on methyl orange dye under UV light and reported 93.76% efficiency [14]. Chamanehpour E et al., (2022) prepared g-C₃N₄@Cu/ZIF-8

nanocomposite and observed its photocatalytic property in removing carbon-di-oxide about 82.1% and reported it as stable material after 5 cycles [15]. Sayadi MH et al., (2022) fabricated nano adsorbent i.e. γ -Fe₂O₃/MWCNTs/Cellulose, and reported its absorption ability of malachite green dye as 99% [16]. The important thing to be noted in this work is solid dyes from the reed mat industries of veeravanallur are collected, mixed with the normal water from which they prepare the dye solution for industrial purposes, and tested for its degradation in TiO₂ as photocatalyst. Malachite Green (MG), an extensively used cationic, water-soluble dye for the textile industry, known as N-methyl-di-amino-tri-phenyl-methane, is reported as more hazardous [17]. It is one of the most commonly used dyes in manufacturing industries [18] their presence in consuming water leads to extreme irritation, and adverse effects on the kidney, nervous system, respiratory system, and brain [19,20]. In viewing the quote "Sewage can lead to another disaster, which is the disease" by American sociologist Walter Maestri, treating those dye waste is one of the most required needs. Therefore researchers are keen on treating the dye-contaminated water by various techniques such as sedimentation, filtration, coagulation, and flocculation [21]. Because of the bio-persistent nature of dyes these above techniques are not able to treat them, photocatalysis using semiconductor catalyst is more advantageous owing to its complete mineralization of the dye into CO₂ and H₂O, eco-friendly and low requirement of catalyst [22,23]. Because of the sturdy degradation of toxic contaminants under light (photo) illumination titanium-di-oxide has been insistently scrutinized in sterilizing toxic materials [24,25].

Titanium dioxide (TiO₂) is a promising semiconductor material with many excellent properties like innocuous, longevity, economical etc. [26] Rutile, brookite and anatase are the three different forms of titanium-di-oxide on nanoscale with bandgap 2.98eV-3.0eV, 3.26eV and 3.05eV-3.2eV [27, 28, 29]. TiO₂ came out with excellent use in batteries, capacitors, solar cell fabrication, photocatalysis, etc., while there increase in deflection in the energy problem. Amidst these uses, TiO₂ is employed in photocatalysis because of its charge movability, appropriate band gap, and photoreaction [30]. It has been captivating much attentiveness as a consequence of the splitting and removal of pollutants from water and air [31]. Especially, TiO₂ in the anatase phase is utilized in

solar energy conversion owing to its outrageous sensitivity when exposed to light (Photo) [32]. It can catalytically break down adulterants in water from household and commercial waste.

In this work, titanium-di-oxide nanoparticles (catalyst) under four different pH values were synthesized by exploiting the microwave irradiation technique. The samples were characterized by XRD, SEM, HRTEM, XPS, UV-Vis, FTIR, and PL. As an application of this work to society, photocatalytic degradation of the Malachite Green dye under visible light (photo) irradiation with different initial concentrations and pH values are investigated.

MATERIALS AND METHODS

Synthesis of TiO₂ with different pH values

All the required raw materials are purchased from Merck and it is of AR grade. Titanium tetrachloride was the precursor used as a metal (titanium) source, ethylene glycol and urea were also used for synthesis. Titanium tetrachloride and urea in the fixed ratio were mixed well in ethylene glycol as a solvent for about 1 hour. The entire solution was poured into a ceramic bowl and treated in a microwave oven at a regular interval of 60 sec/cycle. The substance which is left after the complete evaporation of the solvent is collected, cleaned with double distilled water about four to five times to remove the impurity materials present in the final product, filtered, and dried in a hot air oven at 70°C for five hours. To revamp the crystallinity, the sample was annealed at 475°C for two hours by placed in a muffle furnace [33].

Characterisation Technique

A digital pH meter with ATC Glass Electrode, MP1 plus Sushima is used to measure the pH value of Ethylene Glycol (solvent) during synthesis. The synthesized samples are characterized for the structural properties through powder X-ray diffraction (XRD) using XPERT-PRO spectrometer with CuK α radiation ($\lambda = 1.54 \text{ \AA}$) in powder form of sample, Scanning Electron Microscope (SEM) Micrograph is recorded using VEGA3 TESCAN, High-Resolution Transmission Electron Microscope (HRTEM), SAED and EDAX using JOEL (JEM-2100) Electron Microscope by coating the sample in a copper grid, elements electronic state using PHI - VERSAPROBE III - X-ray Photoelectron Spectroscopy (XPS) in powder form of sample, optical properties through

Fourier Transform Infrared Spectroscopy (FTIR) using FT-IR Nicolet IS5R FTIR, KBR Windows with AR Diamond Crystal Plate with samples in powder form, absorbance spectra using UV-Visible Spectrophotometer, Double beam, make UH-5300, Photoluminescence (PL) using Varian Cary Eclipse Photoluminescence spectrophotometer. The photocatalytic application of the synthesized sample is studied by using a temperature-controlled condenser setup.

2.3 Photocatalytic Experiment

Photocatalytic Degradation of the malachite green dye in the presence of Titanium-di-oxide as a catalyst under irradiation of visible lamp with respect to time is observed first. Initially, the four pH varied catalyst (TiO₂) of 50 mg is measured and made to stir in dark along with the dye solution made out of the freshwater used in the reed mat industries in the veeravanallur area for about 1 hour. As a next step, the entire solution was placed in the dark chamber, illuminated with a visible lamp, and stirred continuously using a magnetic stirrer [34]. Then the photocatalytically treated dye water is at a regular interval of 15 min and tested for its degradation efficiency. The nanocatalysts are also tested for malachite green dye degradation with 50mg catalyst, and dye solution at pH-7, the temperature of the photocatalytic chamber is maintained at room temperature and by varying the initial concentration of dye solution ranging from 100ppm to 400ppm. pH value of the dye solution is varied for both acidic and basic nature. The same amount of nanocatalyst (50mg) is added to the dye solution subjected to various pH conditions. 1M of HCl and NaOH solution is utilized to diverge the pH value of the dye solution. Other parameters like initial dye concentration (100 ppm), photocatalytic chamber temperature (room temperature), and visible light source are kept constant all over the examination of dye degradation using TiO₂ as a catalyst. A cyclic test for the catalyst synthesized under pH-12, which is our best photocatalyst, is analyzed. The same procedure is repeated as mentioned before, with the catalyst load of 50mg in 100ppm of dye solution having a neutral pH i.e. pH-7 under room temperature in 90 min. For each cycle, samples are washed in double-distilled water and acetone 10 times and dried for 5 hours to detach the dye adsorbed in the catalyst [35]. The reusability performance is carried out five times with the same catalyst resulting in a mild decrease in its photocatalytic activity.

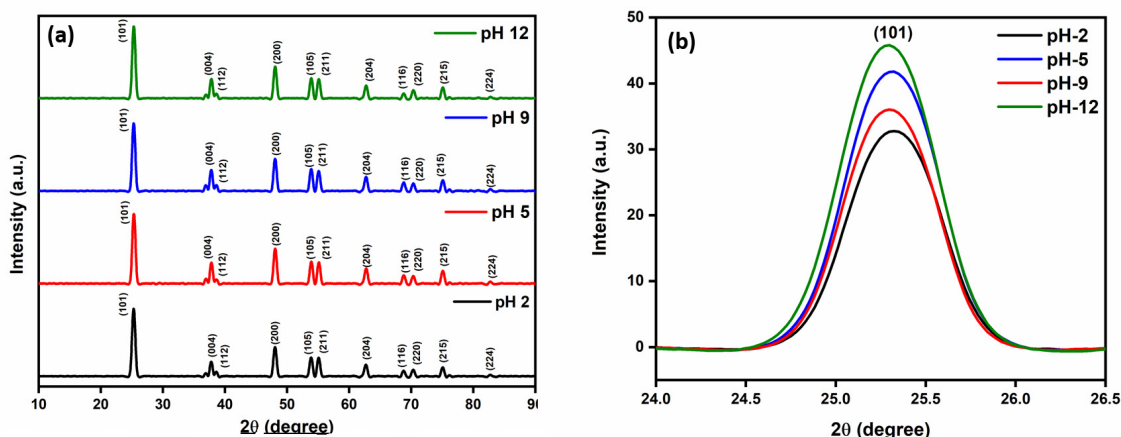


Fig. 1. (a) XRD spectra of TiO₂ synthesized at various pH conditions, (b) dominant peak of XRD spectra

Table 1. Ratio of initial and final product with time period.

Samples	Titanium Tetrachloride (l)	Urea (g)	Ethylene Glycol (ml)	Weight of the final product(g)	Time Taken for synthesis (min)
pH-2	18.968	18.018	100	10.70	6
pH-5	18.968	18.018	100	11.72	9
pH-9	18.968	18.018	100	9.16	11
pH-12	18.968	18.018	100	8.95	14

RESULT AND DISCUSSION

XRD Analysis of TiO₂ nanoparticles

XRD patterns of the pH-varied TiO₂ nanoparticles are shown in Fig. 1(a). The anatase phase of the synthesized TiO₂, peak position, and their intensities agree with the Joint Committee on Powder Diffraction Studies (JCPDS) card using X'pert high score software. The dominant peak arises at 25.5° with the corresponding plane at (101) [36]. Other peaks were spotted at 38°, 48°, 53°, 55°, 62°, 70°, 75°, and 82° [37] with their respective Miller indices at (004), (112), (200), (105), (211), (204), (220), (215) and (224) ascribing the anatase phase, tetragonal crystal system with the space group of I4₁/amd [38]. The achievement of better electron transfer and adsorption of dye is due to this pure anatase form [39]. There was an increase in peak intensity with the increase in pH value (Fig.1 (b)) ascribing the increase in crystalline size. The average crystalline size for 2, 5, 9, and 12 pH-varied synthesized TiO₂ is calculated as 23.87nm, 24.26nm, 26.54nm, and 27.62nm from the Debye-Scherrer equation with the Scherrer constant of 0.94 [40]. During chemical synthesis, pH may alter the synthesis time and size of the nanoparticles, agglomeration of particles occurs with an increase

in reaction time leading to increasing in crystalline size. Table 2 provides the JCPDS file, lattice parameters a, b, and c, volume of the cell, and crystalline size. The lattice parameters a, b, c, and volume of the cell is calculated by using equation 1(a) and 1(b),

$$\frac{1}{d_{hkl}^2} = \frac{(h^2 + k^2)}{a^2} + \frac{l^2}{c^2} \tag{1(a)}$$

$$V = a^2c \tag{1(b)}$$

SEM and EDAX Analysis

For the application in dye degradation, pure TiO₂ nanoparticles were tested for morphological analysis. Fig. 2(a) gives the Scanning Electron Microscope image of the pH-varied synthesized TiO₂ at pH 12. It provides an SEM image of TiO₂ with a granular size of about 27nm [44]. Plate-shaped grains are found from SEM analysis. Their high surface area in this plate form helps in promoting the photocatalytic activity of the catalyst. The presence of titanium and oxygen is confirmed by the X-ray Electron Diffraction Analysis. Since the study is made by coating

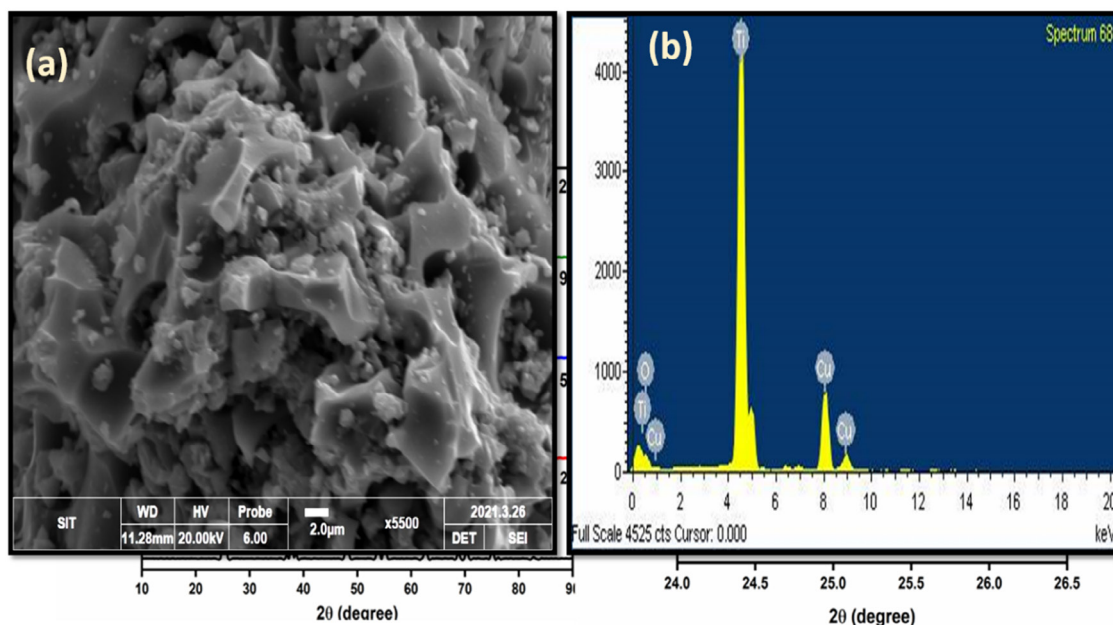


Fig. 2. (a) SEM image of TiO₂, (b) EDAX representation of TiO₂

Table 2. JCPDS File, Lattice parameter, Volume of the cell and Crystalline Size of TiO₂ at pH 2,5,9,12 on annealed at 475°C.

Sample	JCPDS File	Lattice parameters				Volume of the cell (Å ³)		Crystalline Size (nm)	Reference
		Standard Value (Å)		Calculated Value (Å)		Standard Value	Calculated Value		
		a=b	c	a=b	c				
pH 2	01-071-1167	3.7892	9.5370	3.7853	9.51964	136.93	136.41	23.87	
pH 5	01-071-1166	3.7842	9.5146	3.7832	9.5148	136.25	136.18	24.26	
pH 9	01-084-1285	3.7848	9.5124	3.7806	9.5158	136.26	136.01	26.54	[33, 34, 35]
pH 12	01-071-1166	3.7842	9.5146	3.7838	9.5187	136.25	136.28	27.62	

Table 3. EDAX Parameters from Figure 2 (b)

Element	Weight (%)	Atomic (%)
O K	0.89	2.82
Ti K	71.21	75.02
Cu K	27.90	22.16

synthesized nanopowders in a copper grid there are some peaks representing copper are present. Table 3 shows the weight percent and atomic weight percent of TiO₂ using EDAX spectra. Fig. 3(a) provides the HRTEM morphological analysis of Titanium-di-oxide nanoparticles. Following the histogram from Fig. 3 (b), 25.97nm was the particle size obtained with the standard deviation value of about 4.65nm which is similar to the crystalline size obtained from XRD analysis. The distribution of particles in the nanometre range is attested by this HRTEM analysis [45]. In the SAED portrait (Fig. 3 (c)), the diffraction patterns are designated

to their respective crystalline planes (101), (200), (105), (204), (220), and (215) of anatase state [46]. The interplanar spacing d_{hkl} matches well with the JCPDS file: 01-071-1166 from XRD analysis. Both the HRTEM and SAED analysis are in tune with the XRD report.

Chemical States Analysis

To validate the existence of an electronic state of elements and binding energy XPS analysis is studied. Fig. 4(a) portrays the survey scan of the TiO₂, corresponding peaks of Ti 2p and O 1s are revealed in this figure. The anatase titania is shown

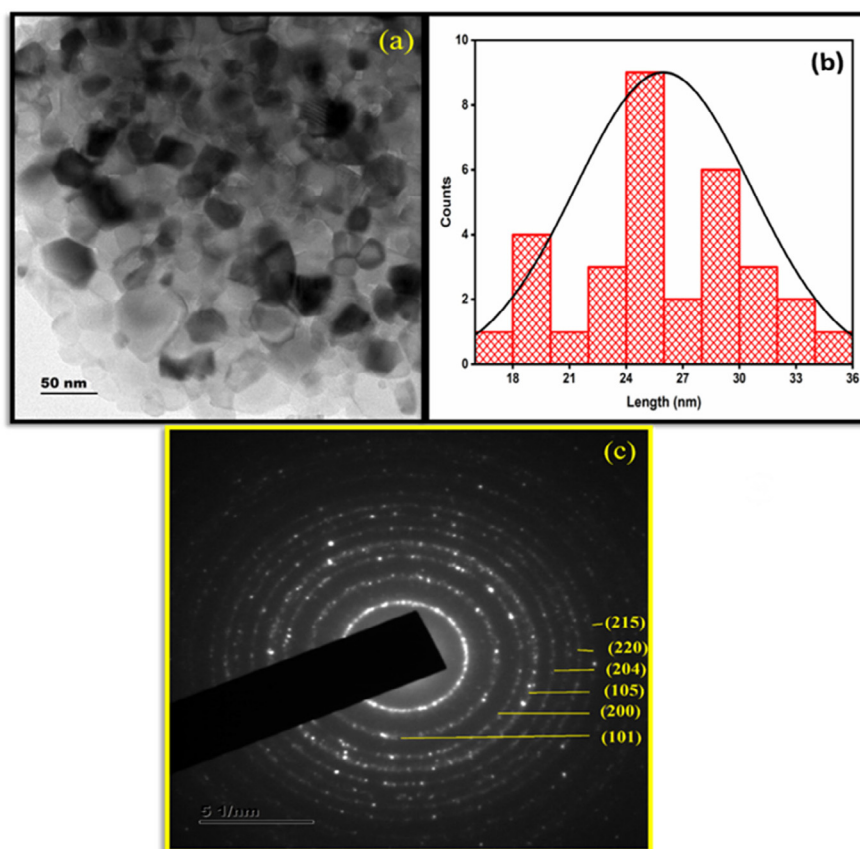


Fig. 3. (a) HRTEM image of TiO_2 nanoparticles (b) Particle Size graph of TiO_2 Synthesized under pH -12 condition

by the Ti 2p plot with two peaks around 457.2 eV, 462.95 eV of $3/2$, $1/2$ can be ascribed to $\text{Ti } 2p_{3/2}$ and $\text{Ti } 2p_{1/2}$ respectively labeling the Ti^{4+} in TiO_2 . [47, 48]. The peaks $\text{Ti } 2p_{3/2}$ and $\text{Ti } 2p_{1/2}$ are at a distance of 5.75 eV which is in agreement with the standard distance in the binding energy of Ti 2p (Fig. 4 (b)) [49]. The pure Titania anatase phase is well agreed with the previous report [50]. The O1s peak (Fig. 4 (c)) is spotted at 528.4 eV which is attained to oxygen bonded with titania ions and 531.1eV is assigned to the vacancy of oxygen boosting up the semiconductor oxide's photocatalytic action [51]. The atomic percentage from this analysis is reported for Ti 2p and O 1s as 22% and 78%. This reveals oxygen-rich TiO_2 , which aids in elevating photocatalytic activity under visible light [52].

Fourier Transform Infrared Analysis

FTIR analysis of TiO_2 nanoparticles is observed in the range 4000 cm^{-1} - 400 cm^{-1} . Fig. 5 depicts the FTIR spectra of the four pH-varied synthesized nanoparticles. In the four pH variation, a broad

transmittance band in the region of 900 cm^{-1} to 400 cm^{-1} is assigned to vibrations of Ti-O-Ti interconnection and the peak at 432 cm^{-1} might be due to the TiO_2 (anatase) vibration mode of Ti-O linkage [53].

Optical Absorption and Bandgap Analysis

To find the optical bandgap, UV-Vis absorbance spectra are measured in the ranges from 200nm to 800nm. Fig. 6 (a) shows the UV-Visible absorption spectra of pH- modified TiO_2 nanoparticles. The optical absorption edge of pH-2 modified TiO_2 is 426nm while with pH -12 modified TiO_2 is 434nm. A minute redshift is noted in this case which might be ascribed to the surface modification of TiO_2 . [54] Which in turn can boost the photocatalytic nature of TiO_2 below visible light, and more charge carriers can be produced. This shift in the UV spectrum might be the reason for the difference in the optical bandgap. The bandgap of the synthesized nanoparticles is deduced by sketching $(\alpha h\nu)^2$ versus $(h\nu)$. On extending the plot, (Fig. 6 (b, c, d,

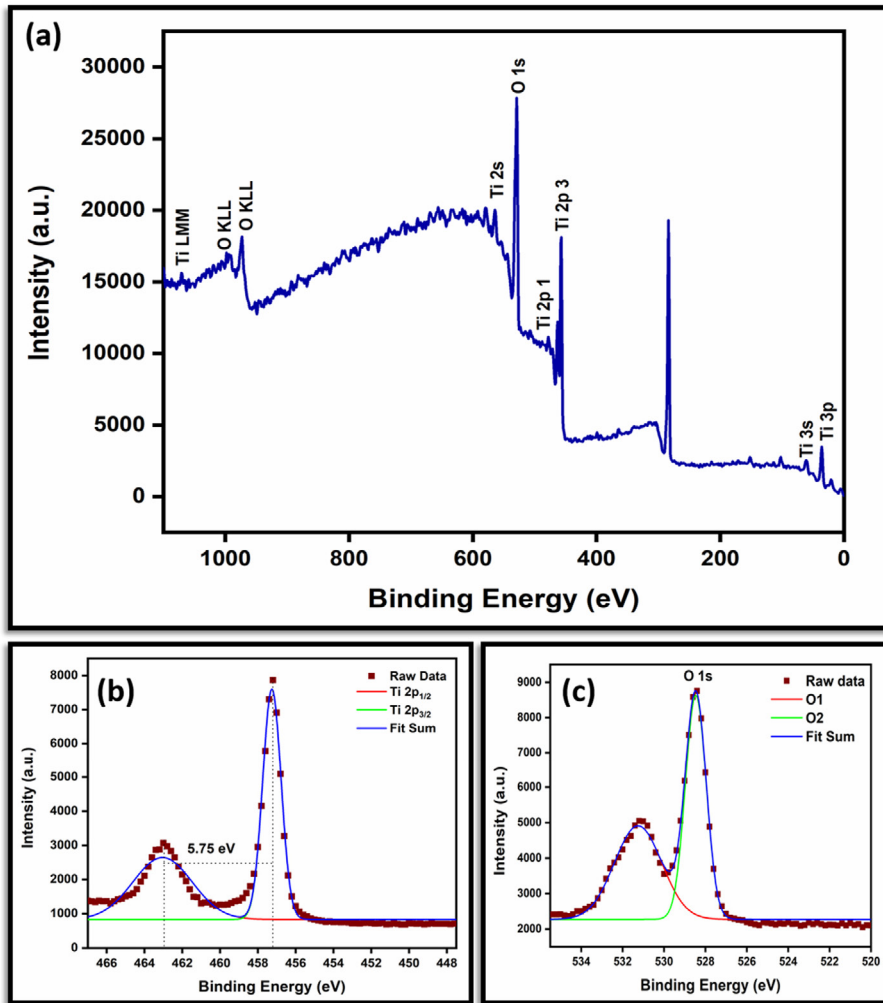


Fig. 4. (a) Survey scan of TiO_2 nanocatalyst, (b) XPS spectra of Ti 2p, (c) XPS spectra of O 1s.

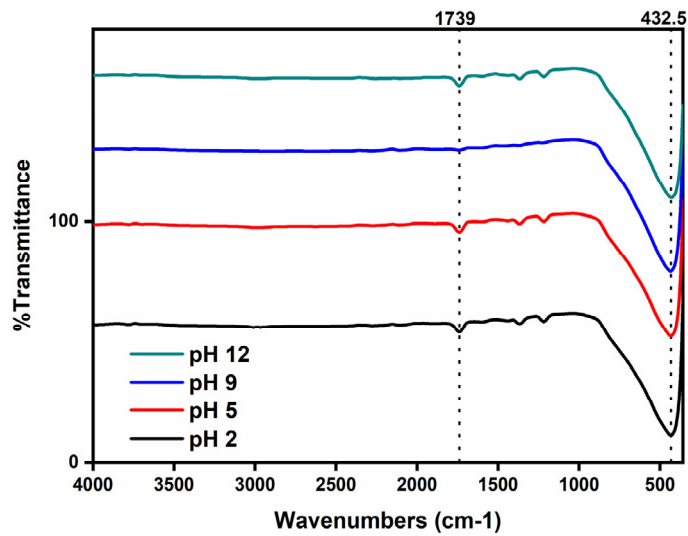


Fig. 5. FTIR spectra of TiO_2 nanoparticles

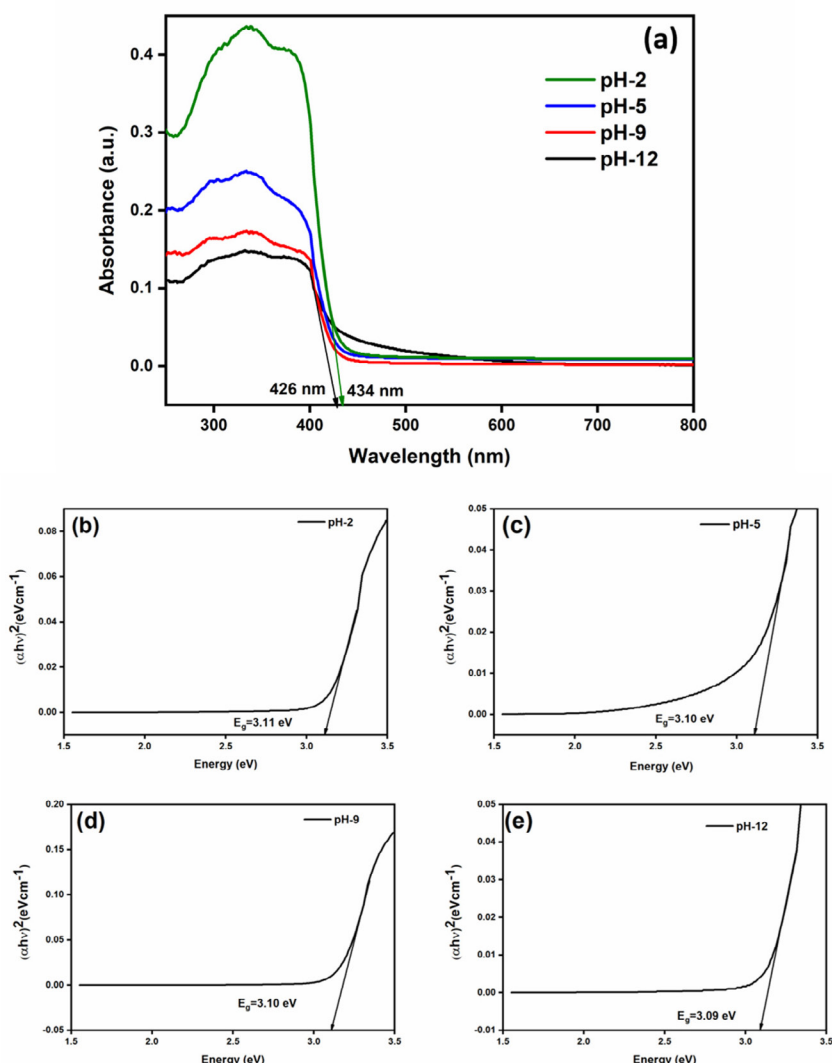


Fig. 6. (a) UV-Vis absorbance spectra of TiO₂ photocatalyst, Band gap plot of TiO₂ synthesized under (b) pH-2, (c) pH-5, (d) pH-9 and (e) pH-12

e) direct bandgap of the material is computed as 3.11eV, 3.10eV, 3.10eV and 3.09eV [55]. It is noted that there is a decrease in bandgap with an increase in the pH of the solvent. By comparing all the samples, it is distinguished that TiO₂ synthesized under pH-12 showed higher absorbance and a small optical bandgap. The tapering of bandgap energy also affirms the oxygen-rich nature of the sample enhancing its photocatalytic properties [56]. The value of absorbance (A), absorption coefficient (α), and absorbance depth (δ) are computed and cataloged in Table 4 using equation 2 (a) and (b) the relation [57]

$$\alpha = \frac{2.303 \times A}{t} \text{ cm}^{-1}, \quad 2(a)$$

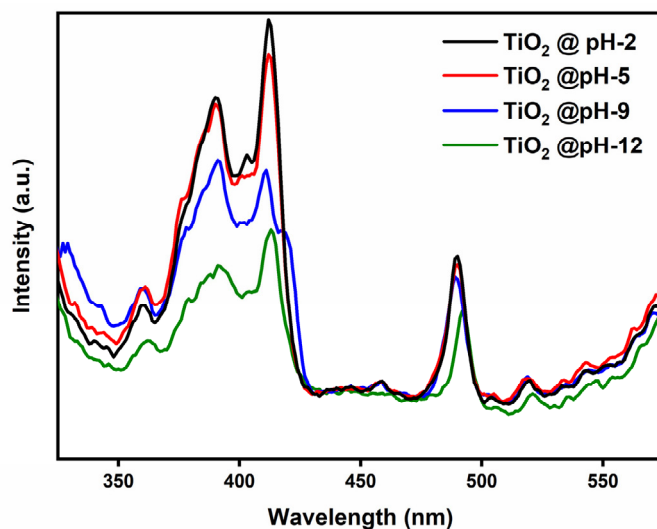
$$\delta = \frac{1}{\alpha} \text{ cm} \quad 2(b)$$

Photoluminescence Analysis

In semiconductor particles, to acknowledge the destiny of hole/electron pair photoluminescence spectra have been intensively used. PL spectrum depends on precursor materials, the solvent used, time taken for synthesis, annealing temperature, and surrounding conditions [58]. For determining the

Table 4. UV-Vis absorbance, Absorption coefficient (α) and absorption depth (δ) of four microwave assisted synthesized TiO₂ Nanoparticles:

Sample	Absorbance (a.u.)	Absorption Coefficient (α) cm ⁻¹	Absorption Depth (δ) cm
pH-2	0.148	0.3408	2.9343
pH-5	0.172	0.3961	2.5246
pH-9	0.242	0.5573	1.7944
pH-12	0.427	0.9834	1.0169

Fig. 7. Photoluminescence Spectra of TiO₂ synthesized at various pH.

exact excitation wavelength in PL spectra absorption spectra from UV-Vis analysis corresponding to the wavelength of excitation is used. In the current work, the photoluminescence emission analysis spectrum of various pH-controlled synthesized titanium-di-oxide nanopowders with an excitation wavelength of 300nm is sported in Fig. 7. Generally, lower intensity of PL spectra corresponds to higher photocatalytic activity. The absorption spectrum is shifted to shorter wavelengths relating it to the maximum emission spectrum. This shift is named as Stokes shift. There was a decrease in peak intensity is observed when the pH of the solvent during synthesis gets increased, this results in demoting the ratio of electron-hole pair recombination, by overcoming the drawback of rapid recombination of electron and hole pairs promoting the charge carrier separation which results in enhancing dye degradation process in photocatalytic treatment [59]. The visible emission peaks at 489nm, 490nm, and 492nm are attributable to electrons caught in sites of oxygen vacancy. The broad emission peak from 360nm to 430nm rises from exciton recombination.

Photocatalytic Degradation

Effect of Contact Time

Under the illumination of a visible lamp, the dye samples are collected at regular time intervals and tested for dye absorption by the catalyst using UV-Vis Spectrometer. Fig. 8 depicts the UV absorbance curve on degrading the malachite green dye by adding TiO₂ as a catalyst. To determine the degradation efficiency of the malachite green dye using equation 3 following relation

$$\text{Degradation efficiency (\%)} = (A_0 - A_t) / A_0 \times 100 \quad (3)$$

Where A_0 and A_t are the initial and final absorbance of the malachite Green dye is used [60].

Dye solution in the presence of TiO₂ as a catalyst on visible lamp illumination was collected under a regular interval of time. The degradation of malachite green dye goes on increasing as time goes by. The presence of dye molecules gets reduced with an increase in time. It takes about 240 min on degrading the dye with a concentration of 400 ppm. The dependence of time on degrading the malachite green dye for the four samples is sketched

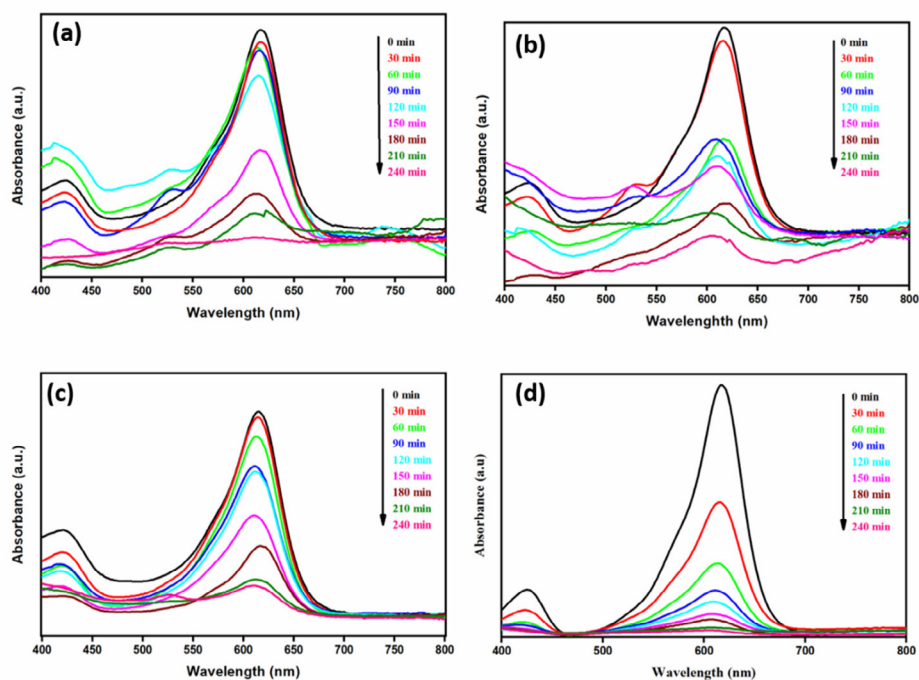


Fig. 8. UV absorbance curve on degrading the malachite green dye on adding TiO_2 as a catalyst.

in Fig. 9(a). The catalyst synthesized under pH-12 condition turns up with the best result of 93.27% within 240 min. Some of the previous literature work on degrading malachite green dye with TiO_2 as a catalyst is compared with current work and tabulated.

Effect of Initial Dye Concentration

The reliance of dye concentration at the initial stage on photocatalytic degradation for all four samples is represented in Fig. 9(b). It is observed that with the increase in the concentration of dye the degradation efficiency by the catalyst drops a little amount. When the concentration of dye increases from 100ppm to 400ppm the degradation efficiency is noted from 96.79% to 93.27%, a decrease in efficiency. The time required for degrading dye solution with varying initial concentrations also gets prolonged. An increase in time was observed on degrading the dye with higher concentration. Electron and hole pair originated upon visible lamp illumination gets lower in count resulting in diminishing the efficiency of degradation [62].

Effect of pH

Initially, the dye solution is made with their appropriate pH values, stirred after adding the catalyst for about one hour in dark. The appearance

of the dye solution is dark in acidic nature upon addition of HCl to it. The appearance of the dye solution looks pale upon the addition of NaOH for its basic nature. The reason is that the excess amount of OH free radicals boosted the degradation efficiency of TiO_2 nanocatalysts. The concentration of MG on the TiO_2 surface is reduced owing to the positive surface of both TiO_2 and dye molecule leading to poor degradation of dye in an acidic state whereas vice-versa happens in the basic state reporting better degradation efficiency. The time factor also gets reduced when the dye solution moves from acid to base state [71]. Fig. 9 (c) delineates the pH vs. degradation efficiency of malachite green dye for the four photocatalysts. The dye waste under neutral pH value exhibited better results when compared to other pH states. Fig. 9 (d) shows the variation of particle size, band gap, and degradation efficiency in degrading malachite green dye. The catalyst with a longer band gap has increased the degradation of dye reducing the rate of recombination of electrons and holes.

Degradation Kinetics

By the photocatalytic reaction principle, a high adsorption range of dye on the surface of the nanocatalyst promotes the degradation process. On taking a look at the degradation rate of MG

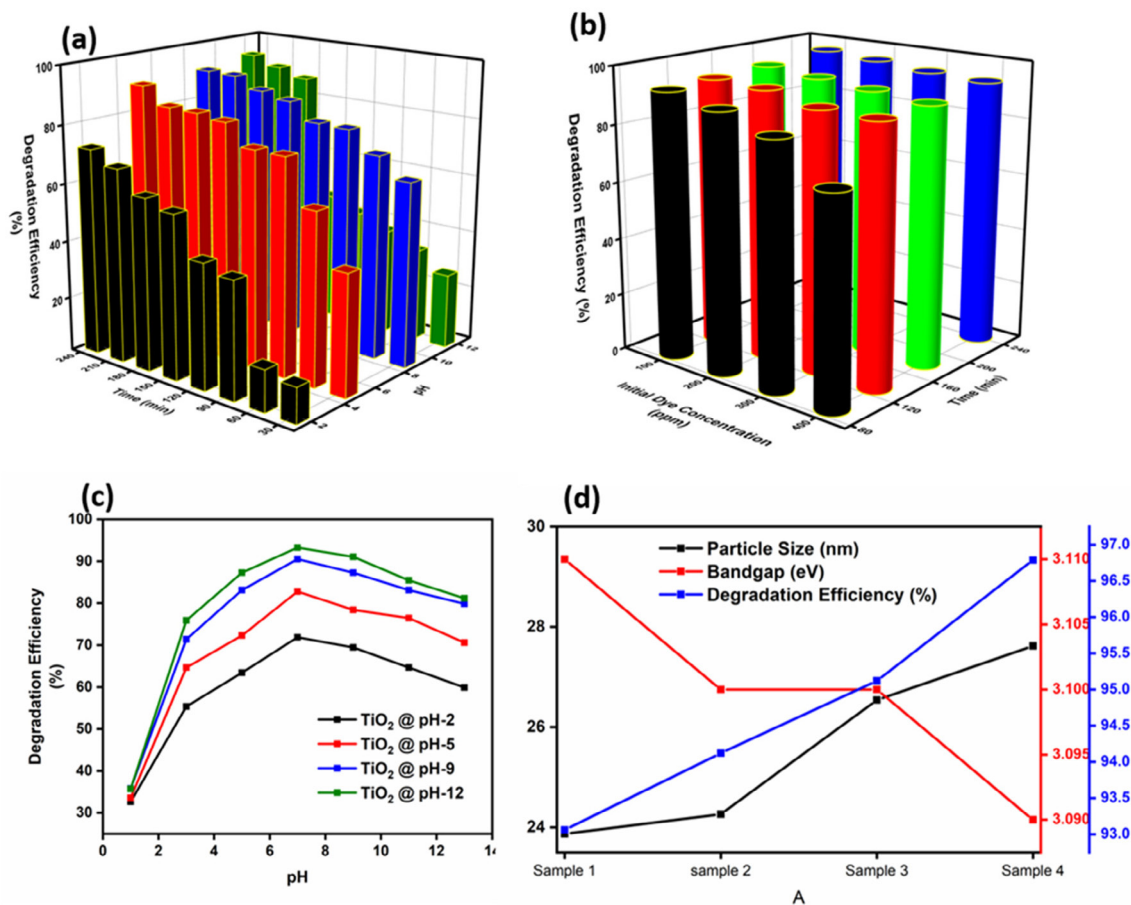


Fig. 9. Dependence of (a)time, (b) initial Concentration, (c) pH on degrading Malachite Green dye with TiO₂ as photocatalyst, (d) Comparison graph of Particle size, Bandgap and photocatalytic degradation efficiency.

Table 5. Comparison of literature work with current work

Catalyst Load(mg/l)	Initial Dye Concentration (ppm)	Time (min)	Degradation Efficiency (%)	Reference
20	20	90	96	[54]
15	5.5	80	99	[55]
5	50	180	70	[56]
-	-	80	90	[57]
-	50	180	93	[58]
500	15	150	98	[59]
600	0.5	60	56	[60]
5	25	200	60	[61]
3	30	40	69	[62]
1000	100	60	54	[63]
50	100	90	96.79	Present work
50	200	130	95.62	Present work
50	300	180	94.00	Present work
50	400	240	93.27	Present work

dye with an initial concentration of 400ppm for the nanocatalyst TiO₂ (50mg), pH-7 in visible lamp irradiation for the reaction time of 240min, Pseudo-first-order reaction kinetics relation $\ln(A_0/A_t)$

$A_t = A_0 e^{-kt}$ where initial absorbance of dye solution A_0 , the concentration of dye collected after regular time interval A_t , time t , rate constant of Pseudo first order k , is used [70]. Pseudo-first order kinetic

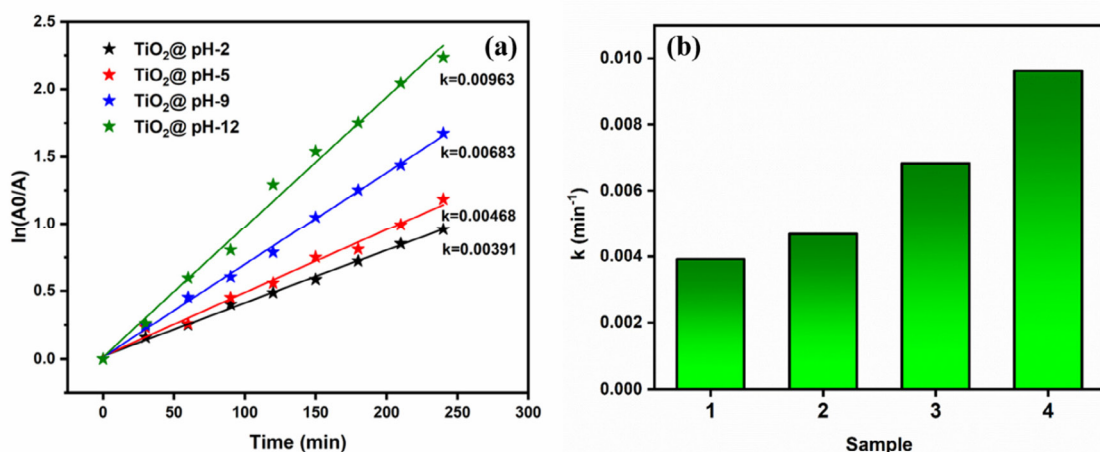


Fig. 10. (a) Pseudo-first-order kinetics plot (b) the kinetic rate constant for all the four samples.

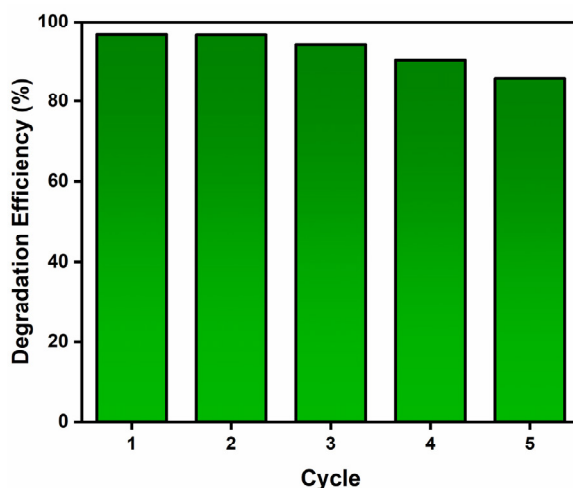


Fig. 11. Reusability and stability for catalytic degradation of pH-12 controlled synthesized TiO₂ nanoparticle.

plot for $\ln(A_0/A)$ Vs. time is plotted in Fig. 10(a). The straight slope from this plot makes us know the first-order rate constant. Through the linear plot, pseudo-first-order rate constants for the four samples are computed as 0.00391min^{-1} , 0.00468min^{-1} , 0.00683min^{-1} and 0.00963min^{-1} and it is plotted, shown in Fig. 10 (b). The nanocatalyst with fine degradation efficiency i.e. nanoparticle synthesized at pH-12 condition reported an increase in reaction rate [72].

Reusability of catalyst

The recyclability and steadiness of the nanocatalyst are key factors responsible for an economical and achievable catalyst. Recycling possibilities of pH-12 controlled synthesized TiO₂ for photocatalytic degradation property are

displayed in Fig. 11. Catalyst, after the recycling process, exhibited a fall in efficiency from 96.79% (1st Run) to 85.78% (5th Run). Considerable stability of the sample is recommended by the result implying a mild fall in degradation during the second cycle. A small depletion in surface photocatalytic activity might be due to the loss of the material during the cleaning process [73]. It may also be due to a decrease in bond strength uniting dye (Malachite Green) and immobilized TiO₂ which can be ascribed to immobilized TiO₂ active sites occupation.

CONCLUSION

Titanium-di-oxide nanoparticles are successfully synthesized under controlled pH conditions via the smart microwave-assisted

solvothermal method. The size of the particle is found to be ranging from 23.87 nm to 27.62 nm using XRD analysis. FESEM and HRTEM also satisfy the particle size from the XRD result. In the pure anatase phase, the elemental composition is confirmed from XPS analysis. The optical bandgap of the four samples is 3.11eV, 3.10eV, and 3.09eV by the tauc plot method. The significance of this work i.e. studying the photocatalytic degradation efficiency of TiO₂ in degrading malachite green dye using the normal tap water from the reed matt industrial areas of veeravanallur is observed by varying dye's initial concentration and the result is outputted that with the increase in concentration there was a decrease in degradation efficiency and the time taken for degrading the dye also increases. In the photodegradation studies taken by varying the pH value of the dye solution, from acidic to alkaline the degradation is speed enough in the base region. Though the neutral pH exhibited a good efficiency. pH-controlled condition of the solvent during synthesis has affected particle size in turn bandgap also have varied, which has enhanced the photocatalytic activity of TiO₂ under visible lamp irradiation reporting an excellent degradation efficiency of 96.79%.

AUTHOR CONTRIBUTION

R. Sarathi- Processed the samples, collected the samples, Data Analysis. Compiled and analyzed the data, writing –original draft, **S. Meenakshi Sundar**-Conceptualization, supervision, validation. All authors have read the final manuscript and confirmed its content.

CONFLICT OF INTEREST

The authors declare no conflict of interest.

REFERENCE

- Rane A, Joshi SJ. Biodecolorization and Biodegradation of Dyes: A Review. *The Open Biotechnology Journal*. 2021 Aug 27;15(1). <https://doi.org/10.2174/1874070702115010097>
- Gičević A, Hindija L, Karačić A. Toxicity of azo dyes in pharmaceutical industry. In *International Conference on Medical and Biological Engineering* 2019 May 16 (pp. 581-587). Springer, Cham. https://doi.org/10.1007/978-3-030-17971-7_88
- Rane A, Joshi SJ. Biodecolorization and Biodegradation of Dyes: A Review. *The Open Biotechnology Journal*. 2021 Aug 27;15(1). <https://doi.org/10.2174/1874070702115010097>
- Ayati A, Ahmadpour A, Bamoharram FF, Tanhaei B, Mänttari M, Sillanpää M. A review on catalytic applications of Au/TiO₂ nanoparticles in the removal of water pollutant. *Chemosphere*. 2014 Jul 1;107:163-74. <https://doi.org/10.1016/j.chemosphere.2014.01.040>
- Dhote J, Ingole S, Chavhan A. Review on wastewater treatment technologies. *Int. J. Eng. Res. Technol*. 2012 Jul;1:1-0.
- Obotey Ezugbe E, Rathilal S. Membrane technologies in wastewater treatment: a review. *Membranes*. 2020 May;10(5):89. <https://doi.org/10.3390/membranes10050089>
- Wong JK, Tan HK, Lau SY, Yap PS, Danquah MK. Potential and challenges of enzyme incorporated nanotechnology in dye wastewater treatment: A review. *Journal of environmental chemical engineering*. 2019 Aug 1;7(4):103261. <https://doi.org/10.1016/j.jece.2019.103261>
- Paździor K, Bilińska L, Ledakowicz S. A review of the existing and emerging technologies in the combination of AOPs and biological processes in industrial textile wastewater treatment. *Chemical Engineering Journal*. 2019 Nov 15;376:120597. <https://doi.org/10.1016/j.cej.2018.12.057>
- Mashkoo F, Nasar A. Magsorbents: Potential candidates in wastewater treatment technology-A review on the removal of methylene blue dye. *Journal of magnetism and magnetic materials*. 2020 Apr 15;500:166408. <https://doi.org/10.1016/j.jmmm.2020.166408>
- Rajabi M, Mahanpoor K, Moradi O. Removal of dye molecules from aqueous solution by carbon nanotubes and carbon nanotube functional groups: critical review. *Rsc Advances*. 2017;7(74):47083-90. <https://doi.org/10.1039/C7RA09377B>
- Panda SK, Aggarwal I, Kumar H, Prasad L, Kumar A, Sharma A, Vo DV, Van Thuan D, Mishra V. Magnetite nanoparticles as sorbents for dye removal: a review. *Environmental Chemistry Letters*. 2021 Jun;19(3):2487-525 <https://doi.org/10.1007/s10311-020-01173-9>
- Dharma HN, Jaafar J, Widiastuti N, Matsuyama H, Rajabsadeh S, Othman MH, Rahman MA, Jafri NN, Suhaimin NS, Nasir AM, Alias NH. A Review of Titanium Dioxide (TiO₂)-Based Photocatalyst for Oilfield-Produced Water Treatment. *Membranes*. 2022 Mar 19;12(3):345 <https://doi.org/10.3390/membranes12030345>
- Sayadi MH, Ghollasimood S, Ahmadpour N, Homaeigohar S. Biosynthesis of the ZnO/SnO₂ nanoparticles and characterization of their photocatalytic potential for removal of organic water pollutants. *Journal of Photochemistry and Photobiology A: Chemistry*. 2022 Mar 1;425:113662 <https://doi.org/10.1016/j.jphotochem.2021.113662>
- Poorsajadi F, Sayadi MH, Hajiani M, Rezaei MR. Photocatalytic degradation of methyl orange dye using bismuth oxide nanoparticles under visible radiation. *International Journal of New Chemistry*. 2021 Jul 1;8(3):229-39 <https://doi.org/10.1080/03067319.2020.1826464>
- Chamanehpour E, Sayadi MH, Hajiani M. A hierarchical graphitic carbon nitride supported by metal-organic framework and copper nanocomposite as a novel bifunctional catalyst with long-term stability for enhanced carbon dioxide photoreduction under solar light irradiation. *Advanced Composites and Hybrid Materials*. 2022 Mar 30:1-7 <https://doi.org/10.1007/s42114-022-00459-6>
- Sayadi MH, Hajiani M, Nowrouzi M. Adsorption studies on the removal of malachite green by γ-Fe₂O₃/MWCNTs/Cellulose as an eco-friendly nanoadsorbent. *Biomass Conversion and Biorefinery*. 2022 Feb 25:1-9
- Sadiq AC, Olasupo A, Rahim NY, Ngah WS, Suah FB. Comparative removal of malachite green dye from aqueous solution using deep eutectic solvents modified magnetic chitosan nanoparticles and modified protonated chitosan beads. *Journal of Environmental Chemical Engineering*. 2021 Oct 1;9(5):106281. <https://doi.org/10.1016/j.jece.2021.106281>
- Swan NB, Zaini MA. Adsorption of malachite green and congo red dyes from water: recent progress and future outlook. *Ecological Chemistry and Engineering*. 2019;26(1):119-32. <https://doi.org/10.1515/eces-2019-0009>
- Sharma S, Kaur A. Various methods for removal of dyes from industrial effluents-a review. *Indian J Sci Technol*. 2018 Mar 1;11:1-21.

- <https://doi.org/10.17485/ijst/2018/v11i12/120847>
20. Pasikhani JV, Gilani N, Pirezabari AE. The effect of the anodization voltage on the geometrical characteristics and photocatalytic activity of TiO₂ nanotube arrays. *Nano-Structures & Nano-Objects*. 2016 Oct 1;8:7-14. <https://doi.org/10.1016/j.nanoso.2016.09.001>
 21. Soo JA, Makhtar MM, Shoparwe NE, Otitouju TA, Mohamad M, Tan LS, Li S. Characterization and kinetic studies of poly (vinylidene fluoride-co-hexafluoropropylene) polymer inclusion membrane for the malachite green extraction. *Membranes*. 2021 Sep;11(9):676. <https://doi.org/10.3390/membranes11090676>
 22. Al-Mamun MR, Kader S, Islam MS, Khan MZ. Photocatalytic activity improvement and application of UV-TiO₂ photocatalysis in textile wastewater treatment: A review. *Journal of Environmental Chemical Engineering*. 2019 Oct 1;7(5):103248. <https://doi.org/10.1016/j.jece.2019.103248>
 23. Weldegebrerial GK. Synthesis method, antibacterial and photocatalytic activity of ZnO nanoparticles for azo dyes in wastewater treatment: A review. *Inorganic Chemistry Communications*. 2020 Oct 1;120:108140. <https://doi.org/10.1016/j.inoche.2020.108140>
 24. Komaraiah D, Madhukar P, Vijayakumar Y, Reddy MR, Sayanna R. Photocatalytic degradation study of methylene blue by brookite TiO₂ thin film under visible light irradiation. *Materials Today: Proceedings*. 2016 Jan 1;3(10):3770-8. <https://doi.org/10.1016/j.matpr.2016.11.026>
 25. Zhu D, Zhou Q. Action and mechanism of semiconductor photocatalysis on degradation of organic pollutants in water treatment: A review. *Environmental Nanotechnology, Monitoring & Management*. 2019 Dec 1;12:100255. <https://doi.org/10.1016/j.enmm.2019.100255>
 26. Kaur T, Sraw A, Wanchoo RK, Toor AP. Visible-light induced photocatalytic degradation of fungicide with Fe and Si doped TiO₂ nanoparticles. *Materials Today: Proceedings*. 2016 Jan 1;3(2):354-61. <https://doi.org/10.1016/j.matpr.2016.01.020>
 27. Abisharani JM, Devikala S, Kumar RD, Arthanareeswari M, Kamaraj P. Greensynthesis of TiO₂ nanoparticles using Cucurbitapepo seeds extract. *Materials today: proceedings*. 2019 Jan 1;14:302-7. <https://doi.org/10.1016/j.matpr.2019.04.151>
 28. Suriani AB, Mohamed A, Mamat MH, Othman MH, Ahmad MK, Khalil HA, Marwoto P, Birowosuto MD. Titanium dioxide/agglomerated-free reduced graphene oxide hybrid photoanode film for dye-sensitized solar cells photovoltaic performance improvement. *Nano-Structures & Nano-Objects*. 2019 Apr 1;18:100314. <https://doi.org/10.1016/j.nanoso.2019.100314>
 29. Jaafar MT, Ahmed LM. Reduced the toxicity of acid black (nigrosine) dye by removal and photocatalytic activity of TiO₂ and studying the effect of pH, temperature, and the oxidant agents. In *AIP Conference Proceedings* 2020 Dec 4 (Vol. 2290, No. 1, p. 030034). AIP Publishing LLC. <https://doi.org/10.1063/5.0027512>
 30. Jeon JP, Kweon DH, Jang BJ, Ju MJ, Baek JB. Enhancing the photocatalytic activity of TiO₂ catalysts. *Advanced Sustainable Systems*. 2020 Dec;4(12):2000197. <https://doi.org/10.1002/adsu.202000197>
 31. Allen NS, Mahdjoub N, Vishnyakov V, Kelly PJ, Kriek RJ. The effect of crystalline phase (anatase, brookite and rutile) and size on the photocatalytic activity of calcined polymorphic titanium dioxide (TiO₂). *Polymer degradation and stability*. 2018 Apr 1;150:31-6. <https://doi.org/10.1016/j.polydegradstab.2018.02.008>
 32. Reddy KR, Karthik KV, Prasad SB, Soni SK, Jeong HM, Raghu AV. Enhanced photocatalytic activity of nanostructured titanium dioxide/polyaniline hybrid photocatalysts. *Polyhedron*. 2016 Dec 14;120:169-74. <https://doi.org/10.1016/j.poly.2016.08.029>
 33. Esakki ES, Sarathi R, Sundar SM, Devi LR. Fabrication of Dye Sensitized Solar Cells using Ixora Macrothyrsa. *Materials Today: Proceedings*. 2021 Jun 13. <https://doi.org/10.1016/j.matpr.2021.05.672>
 34. Munguti L, Dejene F. Influence of annealing temperature on structural, optical and photocatalytic properties of ZnO-TiO₂ composites for application in dye removal in water. *Nano-Structures & Nano-Objects*. 2020 Oct 1;24:100594. <https://doi.org/10.1016/j.nanoso.2020.100594>
 35. Govindaraj T, Mahendran C, Manikandan VS, Suresh R. One-pot synthesis of tungsten oxide nanostructured for enhanced photocatalytic organic dye degradation. *Journal of Materials Science: Materials in Electronics*. 2020 Oct;31(20):17535-49. <https://doi.org/10.1007/s10854-020-04309-3>
 36. Sathyajothi S, Jayavel R, Dhanemozhi AC. The fabrication of natural dye sensitized solar cell (DSSC) based on TiO₂ using henna and beetroot dye extracts. *Materials Today: Proceedings*. 2017 Jan 1;4(2):668-76. <https://doi.org/10.1016/j.matpr.2017.01.071>
 37. Konni M, Dadhich AS, Mukkamala SB. Evaluation of surface changes at the interface between TiO₂ nanoparticles and COOH-MWCNTs on hydrogen adsorption capability. *Nano-Structures & Nano-Objects*. 2019 Apr 1;18:100304. <https://doi.org/10.1016/j.nanoso.2019.100304>
 38. Bhogaita M, Yadav S, Bhanushali AU, Parsola AA, Nalini RP. Synthesis and characterization of TiO₂ thin films for DSSC prototype. *Materials Today: Proceedings*. 2016 Jan 1;3(6):2052-61. <https://doi.org/10.1016/j.matpr.2016.04.108>
 39. Yunarti RT, Isa ID, Dimonti LC, Dwiatmoko AA, Ridwan M, Ha JM. Study of Ag₂O/TiO₂ nanowires synthesis and characterization for heterogeneous reduction reaction catalysis of 4-nitrophenol. *Nano-Structures & Nano-Objects*. 2021 Apr 1;26:100719. <https://doi.org/10.1016/j.nanoso.2021.100719>
 40. Haque FZ, Nandanwar R, Singh P. Evaluating photodegradation properties of anatase and rutile TiO₂ nanoparticles for organic compounds. *Optik*. 2017 Jan 1;128:191-200. <https://doi.org/10.1016/j.ijleo.2016.10.025>
 41. Aldbea FW, Ahmad NI, Ibrahim NB, Yahya M. Effect of increasing pH value on the structural, optical and magnetic properties of yttrium iron garnet films prepared by a sol-gel method. *Journal of sol-gel science and technology*. 2014 Jul;71(1):31-7. <https://doi.org/10.1007/s10971-014-3326-4>
 42. Praveena K, Sadhana K, Srinath S, Murthy SR. Effect of pH on structural and magnetic properties of nanocrystalline Y₃Fe₅O₁₂ by aqueous co-precipitation method. *Materials Research Innovations*. 2014 Jan 1;18(1):69-75. <https://doi.org/10.1179/1433075X13Y.0000000116>
 43. Peymanfar R, Azadi F. Preparation and identification of bare and capped CuFe₂O₄ nanoparticles using organic template and investigation of the size, magnetism, and polarization on their microwave characteristics. *Nano-Structures & Nano-Objects*. 2019 Feb 1;17:112-22. <https://doi.org/10.1016/j.nanoso.2019.01.001>
 44. Naik MM, Naik HB, Nagaraju G, Vinuth M, Vinu K, Viswanath R. Green synthesis of zinc doped cobalt ferrite nanoparticles: Structural, optical, photocatalytic and antibacterial studies. *Nano-Structures & Nano-Objects*. 2019 Jul 1;19:100322. <https://doi.org/10.1016/j.nanoso.2019.100322>
 45. RJ MG, Vidyadharan V, Simon SM, Saritha AC, Biju PR, Joseph C, Unnikrishnan NV. Investigations on the blue luminescence enhancement of organically modified SiO₂-TiO₂-PDMS glass matrix. *Nano-Structures & Nano-Objects*. 2019 Oct 1;20:100377. <https://doi.org/10.1016/j.nanoso.2019.100377>
 46. Ravikumar N, Dilip R, Elango P. Gas sensing nature and characterization of Zr doped TiO₂ films prepared by automated nebulizer spray pyrolysis technique. *Optik*. 2020 Mar 1;206:164347. <https://doi.org/10.1016/j.ijleo.2020.164347>

47. Nagaraj G, Irudayaraj A, Josephine RL. Tuning the optical band Gap of pure TiO₂ via photon induced method. *Optik*. 2019 Feb 1;179:889-94. <https://doi.org/10.1016/j.ijleo.2018.11.009>
48. Potle VD, Shirsath SR, Bhanvase BA, Saharan VK. Sonochemical preparation of ternary rGO-ZnO-TiO₂ nanocomposite photocatalyst for efficient degradation of crystal violet dye. *Optik*. 2020 Apr 1;208:164555. <https://doi.org/10.1016/j.ijleo.2020.164555>
49. Kumar S, Vats T, Sharma SN, Kumar J. Investigation of annealing effects on TiO₂ nanotubes synthesized by a hydrothermal method for hybrid solar cells. *Optik*. 2018 Oct 1;171:492-500. <https://doi.org/10.1016/j.ijleo.2018.06.045>
50. Krishnan VG, Elango P, Ganesan V, Sathish P. pH deeds on structural, optical, electrical and gas sensing performance of TiO₂ nanofilms by automated nebulizer spray pyrolysis technique. *Optik*. 2016 Dec 1;127(23):11102-10. <https://doi.org/10.1016/j.ijleo.2016.09.032>
51. Xu L, Xian F, Zhang Y, Wang W, Qiu K, Xu J. Synthesis of ZnO-decorated SnO₂ nanopowder with enhanced photocatalytic performance. *Optik*. 2019 Oct 1;194:162965. <https://doi.org/10.1016/j.ijleo.2019.162965>
52. Nagaraj G, Irudayaraj A, Josephine RL. Tuning the optical band Gap of pure TiO₂ via photon induced method. *Optik*. 2019 Feb 1;179:889-94. <https://doi.org/10.1016/j.ijleo.2018.11.009>
53. Singh MK, Mehata MS. Phase-dependent optical and photocatalytic performance of synthesized titanium dioxide (TiO₂) nanoparticles. *Optik*. 2019 Sep 1;193:163011. <https://doi.org/10.1016/j.ijleo.2019.163011>
54. Vignesh K, Suganthi A, Rajarajan M, Sakthivadivel R. Visible light assisted photodecolorization of eosin-Y in aqueous solution using hesperidin modified TiO₂ nanoparticles. *Applied surface science*. 2012 Mar 1;258(10):4592-600. <https://doi.org/10.1016/j.apsusc.2012.01.035>
55. Hossain MK, Mortuza AA, Sen SK, Basher MK, Ashraf MW, Tayyaba S, Mia MN, Uddin MJ. A comparative study on the influence of pure anatase and Degussa-P25 TiO₂ nanomaterials on the structural and optical properties of dye sensitized solar cell (DSSC) photoanode. *Optik*. 2018 Oct 1;171:507-16. <https://doi.org/10.1016/j.ijleo.2018.05.032>
56. Etacheri V, Seery MK, Hinder SJ, Pillai SC. Oxygen rich titania: A dopant free, high temperature stable, and visible-light active anatase photocatalyst. *Advanced Functional Materials*. 2011 Oct 7;21(19):3744-52. <https://doi.org/10.1002/adfm.201100301>
57. Horti NC, Kamatagi MD, Patil NR, Nataraj SK, Sannaikar MS, Inamdar SR. Synthesis and photoluminescence properties of titanium oxide (TiO₂) nanoparticles: Effect of calcination temperature. *Optik*. 2019 Oct 1;194:163070. <https://doi.org/10.1016/j.ijleo.2019.163070>
58. Koli VB, Ke SC, Dodamani AG, Deshmukh SP, Kim JS. Boron-Doped TiO₂-CNT Nanocomposites with Improved Photocatalytic Efficiency toward Photodegradation of Toluene Gas and Photo-Inactivation of *Escherichia coli*. *Catalysts*. 2020 Jun;10(6):632. <https://doi.org/10.3390/catal10060632>
59. Acharyulu NP, Srinivasu C, Babavali SE. Synthesis of carbon nano spherical structures and nano composite oxide [TiO₂/SnO₂ (2: 1)] hollow spheres by hydrothermal method and study of characterization with photocatalytic activity. *Materials Today: Proceedings*. 2020 Jan 1;27:1282-8. <https://doi.org/10.1016/j.matpr.2020.02.261>
60. Yang J, Xu X, Liu Y, Gao Y, Chen H, Li H. Preparation of SiO₂@ TiO₂ composite nanosheets and their application in photocatalytic degradation of malachite green at emulsion interface. *Colloids and Surfaces A: Physicochemical and Engineering Aspects*. 2019 Dec 5;582:123858. <https://doi.org/10.1016/j.colsurfa.2019.123858>
61. Bibi S, Ahmad A, Anjum MA, Haleem A, Siddiq M, Shah SS, Al Kahtani A. Photocatalytic degradation of malachite green and methylene blue over reduced graphene oxide (rGO) based metal oxides (rGO-Fe₃O₄/TiO₂) nanocomposite under UV-visible light irradiation. *Journal of Environmental Chemical Engineering*. 2021 Aug 1;9(4):105580. <https://doi.org/10.1016/j.jece.2021.105580>
62. Kamble RJ, Gaikwad PV, Garadkar KM, Sabale SR, Puri VR, Mahajan SS. Photocatalytic degradation of malachite green using hydrothermally synthesized cobalt-doped TiO₂ nanoparticles. *Journal of the Iranian Chemical Society*. 2021 Jun 18:1-0. <https://doi.org/10.1007/s13738-021-02303-y>
63. Stoyanova A, Ivanova N, Bachvarova-Nedelcheva A, Christov C. Synthesis and Photocatalytic Activity of Cerium-Doped and Cerium-Boron co-doped TiO₂ nanoparticles. *Journal Of Chemical Technology & Metallurgy*. 2021 Nov 1;56(6).
64. Liu J, Liu Z, Piao C, Li S, Tang J, Fang D, Zhang Z, Wang J. Construction of fixed Z-scheme Ag₂AgBr/Ag/TiO₂ photocatalyst composite film for malachite green degradation with simultaneous hydrogen production. *Journal of Power Sources*. 2020 Sep 1;469:228430. <https://doi.org/10.1016/j.jpowsour.2020.228430>
65. de Santiago Colín DM, Martínez-Chávez LA, Cuán Á, Elizalde-Peña EA, Rivera JA, Guzmán C, Escobar-Alarcón L, Esquivel K. Sonochemical coupled synthesis of Cr-TiO₂ supported on Fe₃O₄ structures and chemical simulation of the degradation mechanism of Malachite Green dye. *Journal of Photochemistry and Photobiology A: Chemistry*. 2018 Sep 1;364:250-61. <https://doi.org/10.1016/j.jphotochem.2018.06.004>
66. Ma Y, Ni M, Li S. Optimization of malachite green removal from water by TiO₂ nanoparticles under UV irradiation. *Nanomaterials*. 2018 Jun;8(6):428. <https://doi.org/10.3390/nano8060428>
67. Solís-Casados DA, Martínez-Peña J, Hernández-López S, Escobar-Alarcón L. Photocatalytic Degradation of the Malachite Green Dye with Simulated Solar Light Using TiO₂ Modified with Sn and Eu. *Topics in Catalysis*. 2020 Feb 10:1-1. <https://doi.org/10.1007/s11244-020-01240-z>
68. KCC, Prabhu TN, Kiran RS, Krishna RH. Applications of artificial neural network and Box-Behnken Design for modelling malachite green dye degradation from textile effluents using TiO₂ photocatalyst. *Environmental Engineering Research*. 2022;27(1):161-9. <https://doi.org/10.4491/eer.2020.553>
69. Loo WW, Pang YL, Lim S, Wong KH, Lai CW, Abdullah AZ. Enhancement of photocatalytic degradation of Malachite Green using iron doped titanium dioxide loaded on oil palm empty fruit bunch-derived activated carbon. *Chemosphere*. 2021 Jun 1;272:129588. <https://doi.org/10.1016/j.chemosphere.2021.129588>
70. Govindaraj T, Mahendran C, Manikandan VS, Archana J, Shkir M, Chandrasekaran J. Fabrication of WO₃ nanorods/RGO hybrid nanostructures for enhanced visible-light-driven photocatalytic degradation of Ciprofloxacin and Rhodamine B in an ecosystem. *Journal of Alloys and Compounds*. 2021 Jul 5;868:159091. <https://doi.org/10.1016/j.jallcom.2021.159091>
71. Pirsahab M, Hossaini H, Nasser S, Azizi N, Shahmoradi B, Khosravi T. Optimization of photocatalytic degradation of methyl orange using immobilized scoria-Ni/TiO₂ nanoparticles. *Journal of Nanostructure in Chemistry*. 2020 Jun;10(2):143-59. <https://doi.org/10.1007/s40097-020-00337-x>
72. Moosavi S, Li RY, Lai CW, Yusof Y, Gan S, Akbarzadeh O, Chowhury ZZ, Yue XG, Johan MR. Methylene blue dye photocatalytic degradation over synthesized Fe₃O₄/AC/TiO₂ nano-catalyst: degradation and reusability studies. *Nanomaterials*. 2020 Dec;10(12):2360. <https://doi.org/10.3390/nano10122360>